

Article

Novel Pillar[5]arenes Show High Cross-Sensitivity in PVC-Plasticized Membrane Potentiometric Sensors

Monireh Dehabadi ^{1,2} , Elif Yemisci ³, Ahmed Nuri Kursunlu ³ and Dmitry Kirsanov ^{1,*} 

¹ Mendeleev Center, Institute of Chemistry, St. Petersburg University, University Embankment, 7/9, 199034 St. Petersburg, Russia

² Department of Chemical and Petroleum Engineering, Sharif University of Technology, Azadi Ave, Tehran 1458889694, Iran

³ Department of Chemistry, Faculty of Sciences, Selçuk University, Konya 42031, Türkiye

* Correspondence: d.kirsanov@gmail.com

Abstract: In this study a variety of novel symmetrically and asymmetrically functionalized pillar[5]arenes were synthesized, structurally characterized and applied as ionophores in PVC-plasticized membrane potentiometric sensors. During the sensitivity studies it was found that these novel sensors demonstrate pronounced cationic response towards different metal ions in aqueous solutions. A selectivity evaluation revealed that the developed sensors do not possess sharp preferences to particular ions, but offer a broad cross-sensitivity and can be employed in potentiometric multisensor systems.

Keywords: supramolecular chemistry; functionalized macrocycle; synthesis; pillar[5]arene; potentiometric sensor; electrochemical detection; ion recognition



Citation: Dehabadi, M.; Yemisci, E.; Kursunlu, A.N.; Kirsanov, D. Novel Pillar[5]arenes Show High Cross-Sensitivity in PVC-Plasticized Membrane Potentiometric Sensors. *Chemosensors* **2022**, *10*, 420. <https://doi.org/10.3390/chemosensors10100420>

Received: 18 August 2022

Accepted: 11 October 2022

Published: 13 October 2022

Publisher's Note: MDPI stays neutral with regard to jurisdictional claims in published maps and institutional affiliations.



Copyright: © 2022 by the authors. Licensee MDPI, Basel, Switzerland. This article is an open access article distributed under the terms and conditions of the Creative Commons Attribution (CC BY) license (<https://creativecommons.org/licenses/by/4.0/>).

1. Introduction

Pillar[5]arenes with pillar-shaped architecture are an emerging family of supramolecular macrocyclic compounds, consisting of five hydroquinone repeating rings connected by methylene groups at the para-positions and forming special rigid tubular structure with two openings [1–3]. The angle between two bridging C-C bonds is 108°, and central cavity size is 4.7 Å [4]. Their descriptive pillararene name was given by Tomoki Ogoshi and coworkers in 2008; his research group was the first to report the synthesis and crystal structure of 1,4-dimethoxybenzene pillar[5]arene, with a 22% product yield [1]. Pillar[5]arenes can be readily synthesized under Friedel Crafts conditions in conventional organic synthesis [5]. This novel class of macrocycles has attracted an outstanding level of attention and has found diverse applications [3,6]. Benefiting from their unique properties such as easy synthesis, facile functionalization, and excellent binding abilities, pillararene derivatives have provided useful platforms to be utilized for many applications. These include controlled and intracellular drug delivery and release [7–9], small molecules recognition [10], host–guest chemistry [10], medical diagnostics and cell imaging [11], ions sensing [12,13], separation [14], biomolecules detection such as amino acids [15,16], extraction of ions by solvent extraction [17,18] and use in other research areas.

Pillar[n]arenes were introduced in chemistry after other macrocycles (cyclodextrins, calix[n]arenes, cucurbit[n]urils). To a certain extent, pillararenes can be considered as calixarene analogues that are different in monomeric hydroquinone units since they are bridged in para-positions by methylene linkages forming pillar-like conformation, while meta-bridged calixarenes are in basket conformation [4]. The application of macrocycles as recognition elements has a long history. Obviously, the similarity between calixarenes and pillararenes assumes that the latter can be employed for design of metal-binding ligands with diverse applications. Pillar[n]arenes have certain potential advantages compared to their sister macrocycles calix[n]arenes. First, the pillar shape and symmetrical architecture of pillar[n]arenes allow for easy functionalization on one, two, five, ten or twelve arms.

Second, the surrounding of the cavity by multiple alkoxy groups assures a rich electron cloud to a macrocycle. Thus, the rigid and electron-rich structure of pillar[n]arenes enables the binding of small molecules and ions with a host–guest principle.

The formation of stable complexes between pillararene hosts and guest species depends on cationic radius, metal affinity to methoxy group, and central cavity size of the pillararene. Heteroatoms of functional groups (mainly oxygen and nitrogen) contribute chelating sites as recognition units for guests by changing the electronic environment in the macrocycle.

Numerous studies devoted to functionalized pillararenes and their applications can be found in the recent literature. For instance, pillar[5]arene functionalized with phosphine oxides and diglycolamide substituents showed superior efficiency in solvent extraction and separation of uranyl, europium and americium ions [14,19]. In other study, pillar[5]arenes bearing amide and carboxylic groups have demonstrated recognition performance for alkali metal ions. The binding ability with alkali metal cations increased by incorporation of the glycylglycine, additional amide, and carboxylic fragments into the pillararene molecule [20].

Various fluorescent, electrochemical, and colorimetric sensors have been developed by incorporating functional signaling groups into pillararene structures. Water-soluble pillar[5]arene was introduced as fluorescent sensor to detect Fe^{3+} . At the same time, pillararene- Fe^{3+} complex could sense F^- with high sensitivity and selectivity [21]. Similar studies were carried out by Zhang's group by developing single 2-aminobenzothiazole functionalized copillar[4+1]arene with strong blue fluorescence at 432 nm. The fluorescence was quenched in the presence of Fe^{3+} and was restored in the presence of fluoride [22]. On–off–on detection of Hg^{2+} and cyanide was reported by hydroxyquinoline functionalized pillar[5]arene fluorescent chemosensor with high sensitivity and selectivity in aqueous solution. Pillararene- Hg^{2+} complex quenched fluorescence intensity and pillararene- Hg^{2+} - CN^- restored it [23].

Cragg's group incorporated dimethoxy pillar[5]arene into carbon paste electrodes to develop electrochemical sensors to selectively detect clinically important alkali metal ions (Na^+ and K^+) over the physiological concentration range [12]. Shamagsumova et al. developed a biosensor for pesticides based on acetylcholinesterase which was linked to a glassy carbon electrode with carbon black and pillar[5]arene [24]. The same group investigated the deposition of polyaniline-pillar[5]arene onto glassy carbon electrode (GCE) and its electrochemical interaction with Cu^{2+} ions by cyclic voltammetry. The ISE also showed high sensitivity in Cu^{2+} detection in polyvitamin drops [25]. Sun and coworkers demonstrated electrochemical detection of paraquat (a herbicide) using pillar[5]arene-based graphene oxide-modified glassy carbon electrode [26].

In general, the topic of pillararene-based sensing is very popular in the literature and we have indicated here only several typical papers from this research domain, while the available body of literature on this subject is rather large.

Surprisingly, there are not too many reports devoted to the application of pillararenes in potentiometric sensing—one of the very popular sensing platforms due to its simplicity, cost-efficiency and broad sensitivity ranges. Among several reports available in the literature on potentiometric pillararene application, we would like to highlight two papers. Stoikova et al. reported a solid-contact potentiometric sensor based on polyaniline (PANI)-functionalized pillar[5]arene as an ionophore for recognition of Cu^{2+} ions [27]. Kothur and coworkers fabricated a potentiometric sensor for H^+ by incorporation of pillar[5]arene derivative into the PVC membrane of an ion-selective electrode. The potential of the sensor showed non-linear response to pH changes from 1 to 4 [28].

The review on the recent applications of pillar[n]arenes in thin film sensors is given in the work [29].

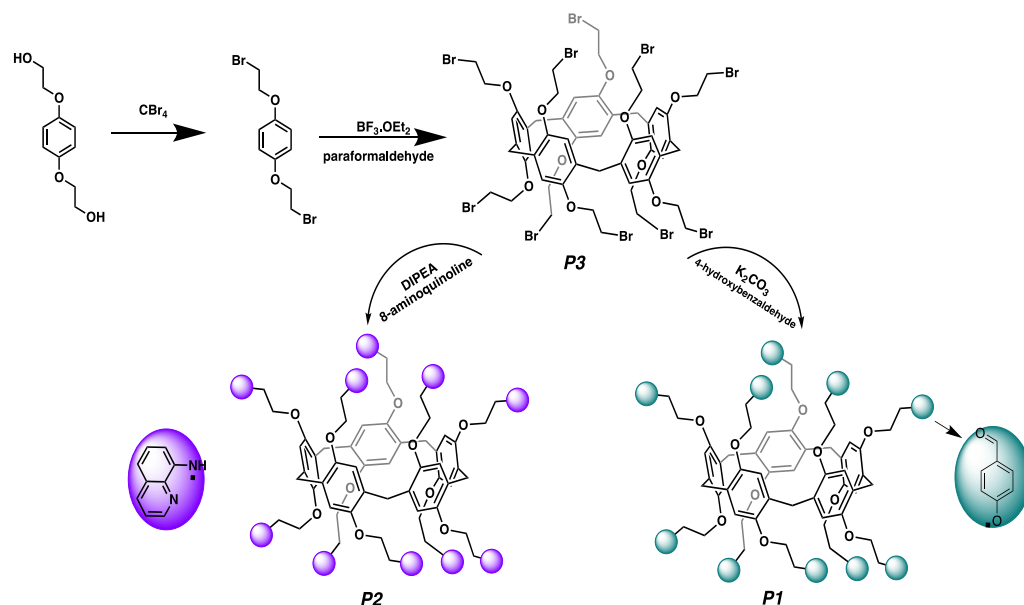
The present study is aimed to further explore the potential of pillar[5]arene derivatives in potentiometric sensing. We report on the synthesis of novel functionalized ligands and their application for metal ions detection in aqueous media. Five pillar[5]arene derivatives

were synthesized in symmetric and asymmetric forms and their potentiometric sensor performance in plasticized polymeric membranes was evaluated. To the best of our knowledge, this is the first investigation on the comparison of plain pillar[5]arene skeletons and their functionalized derivatives for potentiometric detection of metal ions.

2. Materials and Methods

2.1. Synthesis and Characterization of Pillar[5]arenes

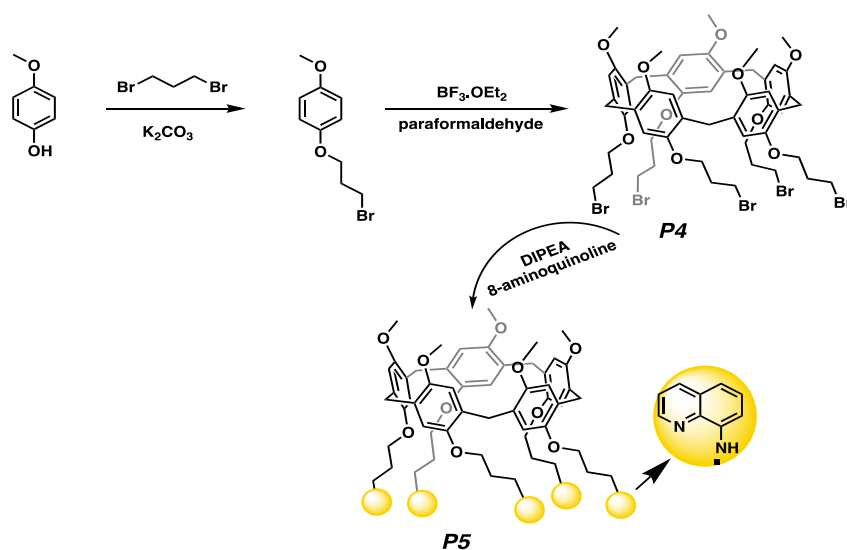
The synthetic routes for symmetric and asymmetric pillar[5]arene derivatives are given in the Schemes 1 and 2. The reactions were carried out under an argon atmosphere. 8-aminoquinoline, carbon tetraiodide, triphenylphosphine, 4-hydroxybenzaldehyde, 1,4-bis(2-hydroxyethoxy)benzene, paraformaldehyde, 1,3-dibromopropane, borontrifluoride etherate, p-methoxyphenol, potassium carbonate, and solvents (1,2-dichloroethane, chloroform, petroleum ether (40–60% dichloromethane, and ethyl acetate) were purchased from Merck (Darmstadt, Germany), Sigma-Aldrich (St Louis, MO, USA) and Acros Chemicals and used without further purification. Characterization of target macrocycles (*P1–P5*) and intermediates was performed by melting point determination, elemental analysis, FT-IR spectroscopy (Bruker Fourier Transform Infrared (ATR)), ¹H-NMR, and ¹³C-NMR (Varian 400 MHz, using of deuteriochloroform or dimethylsulfoxide as solvent) techniques. 1,4-bis(2-bromoethoxy)benzene, 1-(3-chloropropoxy)-4-methoxybenzene, *P1* and *P3* were prepared according to the procedures described in the literature [30–32]. Other pillar[5]arene derivatives were synthesized in several steps with the known organic reactions.



Scheme 1. The synthetic route of symmetric pillar[5]arene derivatives (*P1*, *P2* and *P3*).

2.1.1. The Synthesis of 1-(3-Bromopropoxy)-4-methoxybenzene

1-(3-bromopropoxy)-4-methoxybenzene was synthesized according to the known procedure [30]. 1,3-dibromopropane (4.04 g, 20 mmol) and 4-methoxyphenol (2.48 g, 20 mmol) were dissolved in 80 mL of acetonitrile K_2CO_3 (3 equiv.) and refluxed for 48 h. After the reaction had completed, the residue of heterogenic mixture was removed on filter paper and the solvent was evaporated, producing a pale oil. Yield 3.14 g (77 %). ¹H-NMR (400 MHz, $CDCl_3$, r. t.) δ (ppm): 2.26 (p, 2H, CH_2), 3.66 (t, 2H, CH_2), 3.81 (s, 3H, CH_3), 4.12 (t, 2H, CH_2), 6.86 (d, 2H, PhH), 6.99 (d, 2H, PhH). ¹³C-NMR (100 MHz) δ (ppm): 155.12, 154.15, 116.99, 116.12, 67.75, 56.52, 41.5. Elemental Analysis for $C_{10}H_{13}BrO_2$ Calcd: C, 49.00; H, 5.35; Found: C, 49.14; H, 5.67.



Scheme 2. The synthetic route of asymmetric pillar[5]arene derivatives (**P4** and **P5**).

2.1.2. The Synthesis of **P2** Compound

8-aminoquinoline (1.44 g, 10 mmol) and **P3** (1.68 g, 1 mmol) were dissolved in dry dichloromethane (50 mL), and then 20 mmol of *N,N*-Diisopropylethylamine (DIPEA) were added to this solution. The mixture solution was stirred at room temperature for 48 h by monitoring TLC. Brine solution was added and extraction was performed for three times. The organic phases were collected and dried with Na_2SO_4 . The solvent of the filtrate was removed by evaporator and the pure product was obtained from column by using silica gel (60 mesh) and ethylacetate/40–60%petroleum ether:1/4 eluent. $^1\text{H-NMR}$ (400 MHz, chloroform-*d*, room temperature) δ (ppm): 3.71 (bs, 10H, bridge- CH_2), 3.90 (bs, 40H, CH_2), 5.80 (bs, 10H, NH), 6.98 (bs, 10H), 7.40–7.55 (bs, 40H, PhH), 8.30 (bs, 10H, PhH), 8.72 (bs, 10H, PhH). $^{13}\text{C-NMR}$ (100 MHz) δ (ppm): 20.11, 67.66, 68.99, 105.74, 113.01, 125.33, 125.78, 129.42, 129.79, 130.99, 136.04, 139.70, 145.01, 146.62, 152.03, 160.19. Elemental Analysis calcd. $\text{C}_{145}\text{H}_{130}\text{N}_{20}\text{O}_{10}$: C, 75.30; H, 5.67; N, 12.11 found: C, 75.45; H, 5.89; N, 12.05. m/z calcd for $[\text{M}+\text{H}]^+$, 2313.77; found 2313.66.

2.1.3. The Synthesis of **P4** Compound

Paraformaldehyde (69 mmol, 2.08 g) and 1-(2-bromoethoxy)-4-methoxybenzene (5.61 g, 23 mmol) were dissolved in 1,2-dichloroethane (150 mL). Then, $\text{BF}_3 \cdot \text{OEt}_2$ (1.63 g, 11.5 mmol) was added to this solution using a syringe. It was stirred at r. t. for 3 h under an argon atmosphere. Dichloromethane/water (3×100 mL) were used for the extraction process and dried with sodium sulfate and the filtrate was concentrated in evaporator. The residue was purified in the column (silica gel; petroleum ether/dichloromethane) to obtain **P4** as a white solid (1.89 g, 32%). $^1\text{H-NMR}$ (400 MHz, CDCl_3 , r. t.) δ (ppm): 2.28 (p, 10H, CH_2), 3.65 (t, 10H, CH_2), 3.88 (m, 25H, bridge- CH_2 , CH_3), 4.07 (t, 10H, CH_2), 6.96 (s, 10H, PhH). $^{13}\text{C-NMR}$ (100 MHz) δ (ppm): 14.15, 43.15, 55.67, 65.77, 115.11, 117.05, 131.09, 153.67, 156.5. Elemental Analysis for $\text{C}_{55}\text{H}_{65}\text{Br}_5\text{O}_{10}$, Calcd.: C, 51.38; H, 5.10. Found: C, 51.65; H, 5.52. m/z calcd for $[\text{M}+\text{H}]^+$, 1286.65; found 1286.53.

2.1.4. The Synthesis of **P5** Compound

The synthetic procedure for asymmetric **P5** was similar to that for symmetric **P2** with **P4** as a starting point. $^1\text{H-NMR}$ (400 MHz, chloroform-*d*, room temperature) δ (ppm): 2.28 (bs, 10H, CH_2), 3.65 (bs, 10H, CH_2), 3.88 (m, 25H, bridge- CH_2 , CH_3), 4.07 (t, 10H, CH_2), 5.44 (bs, 5H, NH), 6.96 (s, 10H, PhH) 8.30–8.75 (m, 30H, PhH). $^{13}\text{C-NMR}$ (100 MHz) δ (ppm): 20.11, 43.44, 55.47, 65.88, 68.11, 105.32, 115.45, 117.56, 125.67, 129.67, 131.89, 136.12, 139.45, 153.67, 156.86, 160.39. Elemental Analysis calcd. $\text{C}_{95}\text{H}_{90}\text{N}_{10}\text{O}_{10}$: C, 74.49; H, 5.92; N, 9.14 found: C, 74.33; H, 5.99; N, 9.03. m/z calcd for $[\text{M}+\text{H}]^+$, 1532.83; found 1532.61.

2.2. Potentiometric Sensors Preparation

High molecular weight poly(vinyl chloride) as the polymeric matrix, *o*-nitrophenyl octyl ether (NPOE) or bis(2-ethylhexyl) sebacate (DOS) as polar and non-polar plasticizers, and sodium tetrakis[3,5-bis(trifluoromethyl)phenyl]borate (NaTFPB) as a cation exchanger were procured from Merck (Darmstadt, Germany) in Selectophore[®] grade and used as received. The chemical structures of the employed ligands are shown in Schemes 1 and 2. Analytical-grade tetrahydrofuran (THF) was obtained from Merck (Darmstadt, Germany). Concentrated analytical reagent-grade nitric acid (HNO₃ 65 wt.%) was obtained from Vekton (St Petersburg, Russia). Analytical reagent grade nitrate salts of metals were procured from Sigma Aldrich (Darmstadt, Germany) and were used as received. Standard solutions were prepared by dissolving the appropriate amount of the salts in bidistilled water and then were diluted to the desired concentrations. Freshly bidistilled water from GFL-2102 distillation equipment (GFL GmbH, Hamburg, Germany) was used to prepare the solutions throughout the whole experiment.

The detailed compositions of sensor membranes (in wt.%) are given in Table 1. Polymeric membranes were prepared according to the conventional protocol. Briefly, the components were mixed and dissolved in THF. The solutions were cast into the clean Teflon beakers (ID = 2 cm) and left overnight at room temperature to be dried. The resulting ligand-containing and control dummy membranes (ca. 0.5 mm thickness) were cut into 8 mm circular slices and were glued to the end of PVC tubes (ID = 8 mm, OD = 10mm) as electrode bodies with PVC-cyclohexanone mixture. Electrodes were stored in dry condition at 4 °C prior to use, and were filled with 0.01 M NaCl solution as the internal filling electrolyte and were then conditioned in the same solution for 48 hr prior to measurements. The electrodes were equipped with inner Ag/AgCl electrodes and were connected to the mV-meter. Three identical sensors of each membrane composition were prepared. The compositions with ligands were prepared in three different types: plasticized with NPOE and containing NaTFPB, plasticized with DOS and containing NaTFPB, and plasticized with NPOE without NaTFPB. Besides 15 compositions with ligands, we have also prepared four compositions without ligands for comparison purposes: these were two compositions with NaTFPB plasticized with NPOE and DOS, and two dummy membranes with only polymer and plasticizer.

Table 1. Sensor membrane compositions (wt.%).

| Sensor | Ligand | Polymer Matrix PVC (wt.%) | Plasticizer | | Cation Exchanger NaTFPB (wt.%) | Ionophore Ligand (wt.%) |
|--------|--------|------------------------------|-------------|------------|-----------------------------------|----------------------------|
| | | | NPOE (wt.%) | DOS (wt.%) | | |
| L1 | P1 | 33 | 55.64 | - | 0.88 | 10.45 |
| L2 | P1 | 33 | - | 55.64 | 0.88 | 10.45 |
| L3 | P1 | 33 | 56.52 | - | - | 10.45 |
| L4 | P2 | 33 | 54.55 | - | 0.88 | 11.55 |
| L5 | P2 | 33 | - | 54.55 | 0.88 | 11.55 |
| L6 | P2 | 33 | 55.42 | - | - | 11.56 |
| L7 | P3 | 33 | 57.70 | - | 0.88 | 8.40 |
| L8 | P3 | 33 | - | 57.70 | 0.88 | 8.39 |
| L9 | P3 | 33 | 58.58 | - | - | 8.39 |
| L10 | P4 | 33 | 59.67 | - | 0.88 | 6.42 |
| L11 | P4 | 33 | - | 59.67 | 0.88 | 6.43 |
| L12 | P4 | 33 | 60.55 | - | - | 6.42 |
| L13 | P5 | 33 | 58.45 | - | 0.88 | 7.64 |
| L14 | P5 | 33 | - | 58.45 | 0.88 | 7.64 |
| L15 | P5 | 33 | 59.33 | - | - | 7.64 |
| L16 | - | 33 | 66.09 | - | 0.88 | - |
| L17 | - | 33 | - | 66.09 | 0.88 | - |
| L18 | - | 33 | 67.00 | - | - | - |
| L19 | - | 33 | - | 67.00 | - | - |

2.3. Potentiometric Measurements

The measurements were conducted at room temperature in the galvanic cell setup as follows:

Cu | Ag | AgCl, KCl_{sat} | sample solution | membrane | NaCl, 0.01M | AgCl | Ag | Cu

The sensor readings were registered with KHAN-32 high input impedance multi-channel digital mV-meter (Sensor Systems LLC, St Petersburg, Russia) connected to a personal computer. All sensor potential values were measured with ± 0.1 mV precision against the standard silver/silver chloride reference electrode (EVL-1M3.1 (ZIP, Gomel, Belorussia)) filled with saturated KCl solution. All measurements were performed under the steady stirring conditions on a magnetic stirrer. The duration of the measurements for each sample was three minutes—this was sufficient for reaching the steady readings. The last three sensor potential values recorded within 3 min intervals with 10 s steps were averaged for further data processing. After each measurement, the electrodes were washed with several portions of distilled water to reach the initial potential readings. Sensor responses were recorded in aqueous solutions of inorganic salts in the concentration range from 10^{-8} to 10^{-2} M. All measurements were repeated at least three times to provide for statistical comparison.

2.4. Data Processing

The slope values of the linear part of each calibration curve (measured potential vs. concentration logarithm) were calculated to assess the sensors' sensitivities. All the data were averaged for three identical electrodes in three replicated measurements for each solution. The theoretical Nernstian sensitivities for single-, double- and triple-charged cations are 59, 29, and 19 mV/dec. The higher the slope is, the more sensitive the electrode.

The potentiometric selectivity coefficients $\log K_{ij}^{pot}$ of the studied sensors were evaluated using the bi-ionic potential method (also known as separate solution method) with 10^{-2} M solutions of the primary and interfering ions. In this method, the potential of a cell comprising an ion selective electrode and a reference electrode is measured with two separate solutions. One contains the ion of interest I at the activity a_i (but no j) and the other containing the interfering ion j at the same activity $a_j = a_i$ (but no i), and the selectivity coefficient is derived from the following equation:

$$\log K_{ij}^{pot} = \frac{Z_i F (E_j - E_i)}{2.303 RT} + \left(1 - \frac{Z_i}{Z_j} \right) \log a_i$$

where E_i , E_j and Z_i , Z_j are the respective measured potentials and charges of the ions I and j . The more negative is the $\log K_{ij}^{pot}$, the more selective is the particular sensor towards the given metal (i), and vice versa.

Principal component analysis (PCA) was employed for multivariate data visualization. Briefly, PCA projects the original multivariate space onto a plane determined by two new axes—principal components that represent orthogonal directions of maximal variability in the data. In principle, more orthogonal PCs can be calculated, if needed for visualization. The detailed description of PCA methodology can be found elsewhere [33]. The main outcomes of PCA are scores and loadings plots. The first one indicates similarity/dissimilarity of the samples in the initial multivariate space, while the loadings plot shows the importance of the variables for the observed separation of samples.

3. Results and Discussion

FTIR spectroscopic measurements were performed to examine the organic functional groups of the synthesized ligands. In $^1\text{H-NMR}$ and $^{13}\text{C-NMR}$ spectra, the chemical shifts (δ) were expressed in ppm with internal standard TMS. The FT-IR spectrum of **P3** has some characteristic peaks such as C-O stretching vibration around 1100 cm^{-1} ; C=C multi-vibrations between $1450\text{--}1610\text{ cm}^{-1}$; C-H stretching in the range of $2835\text{--}2970\text{ cm}^{-1}$. After

the synthesis of *P1* and *P2*, these peaks slightly shifted to higher or lower values. Moreover, new stretching bands were observed around 1640 and 1200 cm^{-1} and they can be attributed to C=N vibration in quinoline unit and an etheric C-O-C stretching, respectively. Similar peaks and shifting were detected in FTIR spectra of *P4* and *P5* as they have the same functional organic groups. Thus, the changes in FTIR spectra support the structure of the synthesized compounds (see Figures S1–S3, Supplementary Materials).

The $^1\text{H-NMR}$ spectra of compounds *P1* and *P3* were already interpreted in the literature [34,35]. In $^1\text{H-NMR}$, the protons of 1-(3-bromopropoxy)-4-methoxybenzene appeared at 2.26 ppm (pentet), 3.66 ppm (triplet), 4.12 ppm (triplet) and 3.81 (singlet) for CH_2 and methoxy- CH_3 fragments, respectively. After the synthesis of *P4*, the bridge CH_2 protons were observed to be around 3.88 ppm while other signals raised similar areas, just as the protons in $^1\text{H-NMR}$ of 1-(3-bromopropoxy)-4-methoxybenzene. Then, the transformation of *P5* caused the appearance of new peaks assigned to 8-aminoquinoline. New aromatic signals and NH-proton signals have appeared between 8.60–6.90 ppm and 5.70 ppm, respectively. Similar results were obtained in the transformation of *P3* to *P2* and the peaks were observed in broad singlet forms due to the steric implications of the conformation, and the intermolecular interactions. $^{13}\text{C-NMR}$ spectra were also taken to support the $^1\text{H-NMR}$ spectra of the compounds. The supportive results to the $^1\text{H-NMR}$ spectra were observed in $^{13}\text{C-NMR}$ spectra and showed that the peaks in the aromatic regions generally appeared at values above 110 ppm, while the aliphatic region carbon peaks were in the higher areas. The corresponding spectra can be found in Supplementary materials (Figures S4–S9).

3.1. Sensitivity of Potentiometric Sensors

The synthesized ligands were employed to prepare PVC-plasticized polymeric membranes that were studied as potentiometric sensors. The electrochemical behavior of the sensors was investigated by a potentiometric technique in order to assess their recognition properties towards various metal ions in aqueous media. At first, the fabricated electrodes based on functionalized pillar[5]arenes were studied in the individual aqueous solutions of various metal ions. Typical response curves of the sensors are shown in Figure 1. It can be seen that the sensors demonstrate traditional shapes of potentiometric response typical for cation-sensitive sensors. The standard deviations of the reported sensitivity values did not exceed 2 mV/dec, showing the reproducibility of the responses.

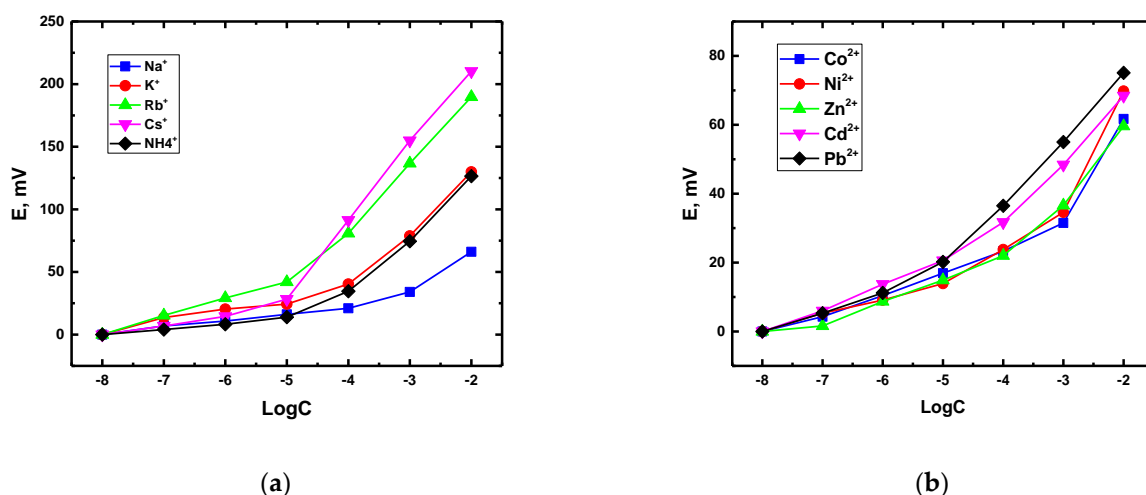


Figure 1. Typical potentiometric response curves: (a) L10 sensors for single-charged cations; (b) L11 sensors for double-charged cations. The EMF readings are offset to zero for better comparability.

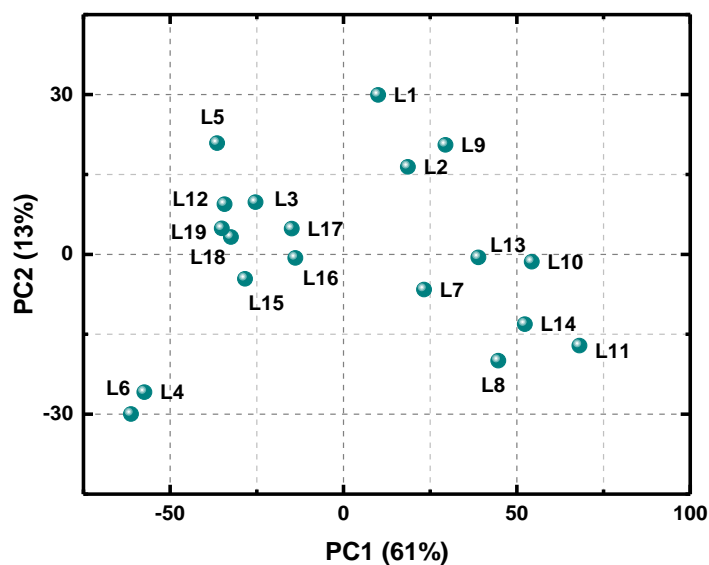
Detailed information on the sensitivity values of the studied sensors towards alkali, alkaline earth, transition metals, and lanthanide ions are presented in Table 2. In order to visualize this large data array, we have employed PCA modeling using sensor types as

samples and sensitivity values towards particular ions as variables. Figure 2 demonstrates the resulted scores and loadings plots.

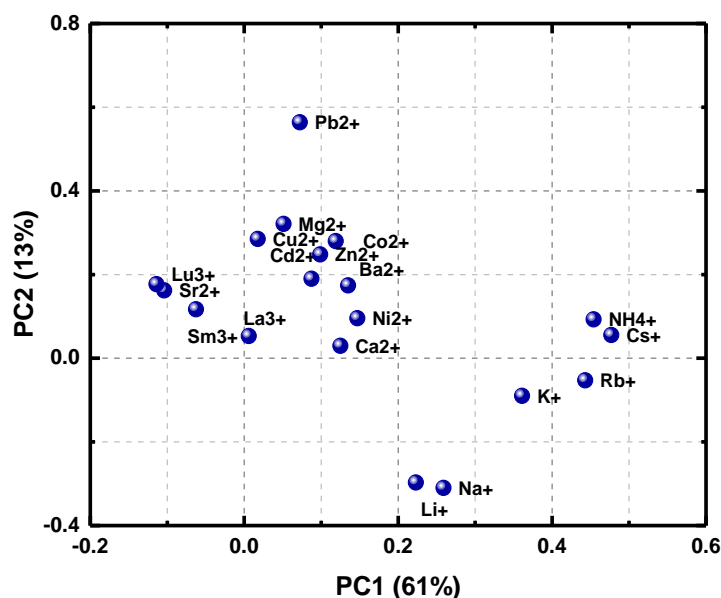
Table 2. Sensitivity values (± 1 mV/dec) of the sensors in aqueous solutions of metal ions. In the case of lanthanides, the measurements were performed at pH 2 (fixed by nitric acid).

| Sensor Number | L1 | L2 | L3 | L4 | L5 | L6 | L7 | L8 | L9 | L10 | L11 | L12 | L13 | L14 | L15 | L16 | L17 | L18 | L19 |
|------------------------------|----|----|----|----|----|----|----|----|----|-----|-----|-----|-----|-----|-----|-----|-----|-----|-----|
| NH ₄ ⁺ | 32 | 47 | 22 | 0 | 16 | 0 | 48 | 54 | 50 | 52 | 56 | 26 | 50 | 52 | 20 | 24 | 22 | 14 | 13 |
| Li ⁺ | 6 | 8 | 8 | 6 | 8 | 5 | 4 | 27 | 13 | 17 | 55 | 8 | 11 | 40 | 11 | 9 | 8 | 7 | 9 |
| Na ⁺ | 16 | 16 | 14 | 15 | 15 | 13 | 13 | 46 | 21 | 32 | 54 | 5 | 21 | 46 | 8 | 16 | 17 | 15 | 15 |
| K ⁺ | 24 | 33 | 17 | 8 | 9 | 8 | 34 | 41 | 36 | 45 | 47 | 11 | 38 | 43 | 11 | 10 | 9 | 9 | 10 |
| Rb ⁺ | 28 | 32 | 7 | 5 | 6 | 0 | 37 | 43 | 37 | 54 | 48 | 6 | 50 | 45 | 9 | 14 | 11 | 9 | 12 |
| Cs ⁺ | 43 | 40 | 17 | 0 | 0 | 0 | 49 | 44 | 37 | 59 | 52 | 7 | 50 | 48 | 11 | 36 | 37 | 9 | 6 |
| Mg ²⁺ | 22 | 26 | 18 | 0 | 21 | 0 | 6 | 10 | 15 | 15 | 15 | 11 | 13 | 13 | 7 | 26 | 0 | 16 | 16 |
| Ca ²⁺ | 10 | 0 | 13 | 0 | 0 | 0 | 11 | 15 | 22 | 18 | 18 | 5 | 17 | 17 | 4 | 18 | 10 | 9 | 13 |
| Sr ²⁺ | 30 | 28 | 26 | 27 | 32 | 30 | 10 | 12 | 16 | 17 | 16 | 4 | 16 | 15 | 5 | 30 | 28 | 30 | 34 |
| Ba ²⁺ | 21 | 18 | 9 | 0 | 2 | 0 | 12 | 15 | 23 | 21 | 16 | 9 | 20 | 16 | 9 | 14 | 19 | 14 | 7 |
| Co ²⁺ | 24 | 21 | 14 | 0 | 19 | 0 | 9 | 12 | 27 | 18 | 30 | 9 | 12 | 15 | 12 | 9 | 13 | 13 | 14 |
| Ni ²⁺ | 11 | 23 | 8 | 0 | 20 | 0 | 10 | 15 | 15 | 22 | 33 | 11 | 17 | 21 | 16 | 0 | 8 | 12 | 14 |
| Cu ²⁺ | 26 | 11 | 29 | 22 | 35 | 0 | 9 | 9 | 28 | 14 | 17 | 13 | 9 | 30 | 6 | 0 | 21 | 16 | 14 |
| Zn ²⁺ | 18 | 14 | 9 | 0 | 24 | 0 | 17 | 15 | 26 | 16 | 19 | 15 | 17 | 15 | 15 | 0 | 14 | 0 | 22 |
| Cd ²⁺ | 15 | 10 | 10 | 0 | 19 | 0 | 12 | 16 | 24 | 16 | 18 | 9 | 15 | 17 | 11 | 12 | 14 | 16 | 16 |
| Pb ²⁺ | 46 | 32 | 25 | 0 | 31 | 0 | 17 | 18 | 29 | 24 | 19 | 25 | 24 | 21 | 23 | 25 | 25 | 25 | 23 |
| La ³⁺ | 4 | 3 | 2 | 0 | 0 | 2 | 0 | 0 | 8 | 0 | 6 | 7 | 1 | 0 | 0 | 4 | 3 | 0 | 3 |
| Sm ³⁺ | 4 | 6 | 10 | 5 | 6 | 7 | 0 | 0 | 12 | 2 | 0 | 12 | 3 | 0 | 5 | 0 | 6 | 9 | 10 |
| Lu ³⁺ | 9 | 11 | 15 | 11 | 11 | 12 | 0 | 0 | 16 | 2 | 0 | 16 | 1 | 0 | 6 | 4 | 10 | 14 | 14 |

There are several factors to be considered when analyzing these data: the influence of the ligand; the influence of the solvent plasticizer (DOS or NPOE); the presence of a cation exchanger (NaTFPB). There is no distinct clustering in the PCA score plot (Figure 2a), however, a certain grouping can be observed. The left-hand side of the score plot has L4 and L6 sensors based on P2 ligand and NPOE plasticizer—these sensors on average have shown the smallest sensitivity values and they have demonstrated practically relevant responses towards Sr²⁺ only. The sensors prepared without the ligands (L16, L17, L18, L19) are also grouped together and the same group contains L3, L12 and L15—the sensors prepared without cation-exchanging additive NaTFPB. The difference between the ligands can be evaluated by calculating the average response values for all sensors based on the same pillar[5]arene. This was done by taking the individual response values of the sensors based on the same ligand in metal ion solutions and dividing their sum by the total number of entries. These calculations yielded the following average slopes: P1 18.2, P2 7.9, P3 20.1, P4 20.6, P5 18.0 mV/dec. Thus, the symmetric P2 with bulky substituents provides for the poorest sensitivity values. This is probably associated with the limited steric availability of the inner molecular cavity of the ligand, which hinders metal ion complex formation. The average sensitivity of the sensors based on other ligands is in general comparable. The sensitivity averaging was also performed for each type of the sensor over all measured ions and the results are given in Table S1 (Supplementary materials). The overall conclusions that can be drawn from this table are the same as above.



(a)



(b)

Figure 2. PCA scores (a) and loadings (b) plot for sensor sensitivities.

The right-hand side of the PCA score plot is occupied by the sensors *L10*, *L11*, *L14* that on average have shown the highest sensitivities towards all metals studied. In this way, *L11* demonstrates near-Nernstian responses towards alkali and some of the transition metals (Co and Ni). Thus, the direction of PC1 in the score plot corresponds to the growth of the average sensitivity (from left to right). As for the PC2, the sensors which have the most different projection values on PC2 are *L1* and *L5* at the upper side, and again *L4* and *L6* at the bottom. *L1* and *L5* have shown the highest sensitivities towards Pb^{2+} , in case of *L1* this value has distinct super-Nernstian character (46 mV/dec). This is well visualized with the loadings plot (Figure 2b), where Pb has the highest loading values along PC2. The location of other variables in the loadings plot indicates that most differences in sensor responses were observed for alkali metals and ammonium, while the response towards

alkali earth and transition metals was comparably homogeneous among the sensors of various composition (the cluster of the corresponding variables is located not far from the coordinate center).

The ligands *P3* and *P4* on average gave the highest sensitivity to alkali metals and ammonium. In the case of alkali earth metals, the best response was obtained from *P1*-based sensors. The same holds for transition metals, however, in this case the difference between *P1*- and *P4*-based sensors was not that much pronounced. As for the lanthanides, in most of the cases the registered sensitivities are not relevant to some practical application as they do not reach theoretical values.

When comparing an average response of the sensors containing NaTFPB with two different plasticizers, one can see that DOS (the average for all compositions is 21.2 mV/dec) outperforms NPOE (17 mV/dec). However, this effect is mainly due to the large difference in responses towards alkali metals, where DOS provides for better sensitivity. This trend is reversed in many cases for transition metals. This agrees well with the common observation that more polar plasticizers (NPOE) promote the response towards doubly charged cations. The influence of the cation exchanger also complies well with traditional potentiometric considerations. On average, the response of the sensors with NaTFPB is higher (17 mV/dec) than without (12.7 mV/dec). The PCA score plot including the third principle component coordinate is given in Figure S10 (Supplementary Materials).

The typical response linearity range for the developed sensors was from 10^{-5} to 10^{-2} M, while the detection limits were around 5.5 pMe. This was valid for the single-charged cations with sensitivity above 30 mV/dec and double-charged cations with sensitivity above 20 mV/dec. The responses of the sensors were stable and reproducible, at least within three months of the experiment with inter day deviations in response slopes not exceeding 1–2 mV/dec.

3.2. Selectivity of Potentiometric Sensors

At the next step of the study, we have explored the selectivity of the developed sensors. Since the sensors have shown a rather broad cross-sensitivity in different groups of metal ions (single and double charged), we found it reasonable to evaluate the selectivity in each group separately. Thus we have measured the selectivity against sodium for alkali metals, against calcium for alkali earth metals and against copper for transition metals. In our opinion, this is more informative than measuring all selectivities against a single ion, e.g., sodium, as in this case we would not be able to obtain a comprehensive picture of sensor performance in different groups of metals. Table 3 shows the values of calculated selectivity coefficients ($\log K_{ij}^{pot}$) from the experimental response curves of the sensors. In order to explore the selectivity in a more detailed way, we have performed separate measurements for each of the ion groups: alkali metals (against Na^+), alkali earth metals (against Ca^{2+}), and transition metals (against Cu^{2+}). Noteworthy, as some of the developed sensor membrane compositions did not show reasonable sensitivities towards particular ions, these compositions were excluded from further considerations.

Among the alkali metals, lithium appears to be the most discriminated ion, while selectivity towards cesium is prevalent for the majority of sensors. The exceptions here are *L2*, *L8* and *L11*, showing quite uniform distribution with no sharp preferences towards particular ions. In the case of alkali earth metals, Ba^{2+} is the most discriminated ion probably due to ionic radius considerations. Sr^{2+} is the preferred ion for the majority of the sensors, except *L1* and *L2* that demonstrate selectivity to Ca^{2+} . It can be noted that among Mg^{2+} , Ca^{2+} and Sr^{2+} , the attained selectivities are also not sharp and the sensors demonstrate a broad cross-sensitivity. Among transition metals lead and cadmium are more preferred by most of the sensors, while there is no strong discrimination among Co^{2+} , Ni^{2+} , Cu^{2+} and Zn^{2+} , where most of the registered selectivity logarithm values are zero. Alkali earth metals except barium were preferred over Cu^{2+} by most of the sensors, but this was not the case for *L14*. Magnesium was preferred over copper by *L8* and *L11*. In general, the developed

sensors have shown a broad variety of selectivity patterns and can be recommended for employment in potentiometric multisensor systems.

Table 3. $\log K_{ij}^{pot}$ values of the studied sensors ($\pm 0.1 \log K_{ij}^{pot}$).

| Sensor Number | L1 | L2 | L7 | L8 | L10 | L11 | L13 | L14 |
|---|------|------|------|------|------|------|------|------|
| NH ₄ ⁺ /Na ⁺ | −0.4 | 0.0 | 0.8 | −0.1 | 0.7 | 0.4 | 1.1 | 0.3 |
| Li ⁺ /Na ⁺ | 0.5 | 0.6 | −3.3 | −1.4 | −0.7 | −0.1 | 0.6 | 0.8 |
| K ⁺ /Na ⁺ | 1.1 | 0.7 | 2.4 | 0.0 | 1.2 | 0.4 | 1.8 | 0.6 |
| Rb ⁺ /Na ⁺ | 1.4 | 0.7 | 1.6 | 0.1 | 1.6 | 0.3 | 2.0 | 0.6 |
| Cs ⁺ /Na ⁺ | 1.4 | 0.3 | 1.9 | 0.2 | 2.1 | 0.5 | 2.6 | 0.7 |
| Mg ²⁺ /Ca ²⁺ | −0.1 | −0.9 | −0.1 | −0.8 | −0.7 | −0.9 | −0.9 | −0.7 |
| Sr ²⁺ /Ca ²⁺ | −1.5 | −2.0 | 0.8 | 0.3 | 0.3 | 0.1 | 0.4 | 0.9 |
| Ba ²⁺ /Ca ²⁺ | −0.6 | −0.6 | 0.8 | −0.1 | 0.9 | −0.1 | 0.9 | 0.1 |
| Co ²⁺ /Cu ²⁺ | 0.2 | −0.2 | 0.6 | −0.6 | 0.0 | 0.1 | 0.4 | −0.9 |
| Ni ²⁺ /Cu ²⁺ | 0.1 | −0.1 | 0.3 | −0.4 | 0.1 | 0.2 | 0.1 | −0.5 |
| Zn ²⁺ /Cu ²⁺ | 0.6 | −0.3 | −0.1 | −0.9 | −0.3 | 0.1 | −0.1 | −1.2 |
| Cd ²⁺ /Cu ²⁺ | 1.5 | 1.2 | 0.7 | −0.3 | 0.2 | 0.2 | 0.8 | −0.7 |
| Pb ²⁺ /Cu ²⁺ | 1.7 | 1.7 | 3.4 | 1.1 | 1.4 | 0.8 | 2.1 | 0.7 |
| Mg ²⁺ /Cu ²⁺ | 1.1 | 0.6 | 3.9 | −0.8 | 0.2 | −0.9 | 0.7 | −1.7 |
| Ca ²⁺ /Cu ²⁺ | 2.8 | 2.3 | 2.3 | −0.1 | 0.9 | 0.4 | 1.2 | −0.5 |
| Sr ²⁺ /Cu ²⁺ | −0.5 | −1.0 | 3.3 | 0.2 | 0.8 | 0.2 | 1.7 | −0.6 |
| Ba ²⁺ /Cu ²⁺ | 0.7 | 0.8 | 3.7 | −0.2 | 1.6 | 0.4 | 1.9 | −0.7 |

Based on the results of sensitivity and selectivity evaluations, it can be seen that the employment of pillar[5]arenes as ligands in plasticized polymeric sensor membranes does not offer sharp selectivity towards particular ions, but offer a broad cross-sensitivity instead. This feature is highly in demand for construction of multisensor arrays—so-called “electronic tongues” [36]. The idea of these systems is based on the application of cross-sensitive sensor arrays combined with chemometric data processing. In this way, the limitations on application of individual ISE associated with insufficient selectivity in complex media can be effectively circumvented. This is a well-established field of research now, and numerous practical applications of such systems have been developed [37–39]. The further studies in this field require novel cross-sensitive sensors with response patterns different from the existing sensors. In this way, the developed pillar[5]arene membranes can contribute to these studies, as their cross-sensitivity patterns are different from a variety of already developed sensors with cationic cross-sensitivity [40–42].

An important and practically relevant feature of potentiometric sensors is their pH-sensitivity, as this may affect the scope of possible applications of the sensors. We have studied this feature. The effect of pH range on the response of the electrodes was determined by gradually changing the pH of the solutions from 12 to 2. The resulting EMF values were plotted against pH of the solutions. The pH of each solution was adjusted using 0.1 M solutions of either HCl or NaOH. Figure 3 illustrates the typical response curves registered in these experiments. Figure S11 (Supplementary Materials) shows the resulted curves for the rest of the developed sensors. The increase in potential at lower pH values indicates that the sensors’ membranes respond to hydrogen ions due to the protonation of the ionophore. It can be seen, that the absence of cation exchanger NaTFPB in membrane composition strongly promotes pH-sensitivity (L3, L9, L12, L15). Most of the sensors demonstrated significant pH response in acidic media. The evaluation of the

response plots shows that the slopes of the pH response curves are lower than theoretical Nernstian values of 59 mV/dec. For example, in the case of *L12* ligand, the overall change in potential for pH window between 3 and 11 is only 200 mV which is equivalent to the response of only 25 mV/pH. This pH sensitivity is comparable with that of various other polymeric membrane sensors and as such it does not preclude the practical application of the sensors; however, this has to be taken into account when considering practical applications of the developed sensors.

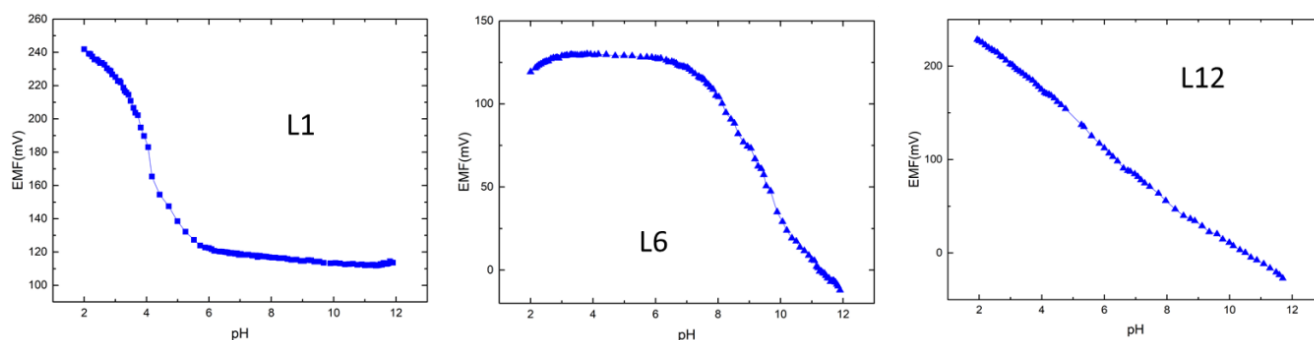


Figure 3. pH-sensitivity of the sensors *L1*, *L6* and *L12*.

The response time of the prepared electrodes was assessed by an injection method according to the IUPAC recommendation. The average time required for the membrane sensor to reach a potential within ± 1 mV or 90% of the final equilibrium (steady-state) value after successive 10-fold addition of analyte concentration was regarded as the response time of each electrode. The dynamic response time of *L10* for Cs^+ is depicted in Figure 4 as an example. Typical response time values were about 5 s.

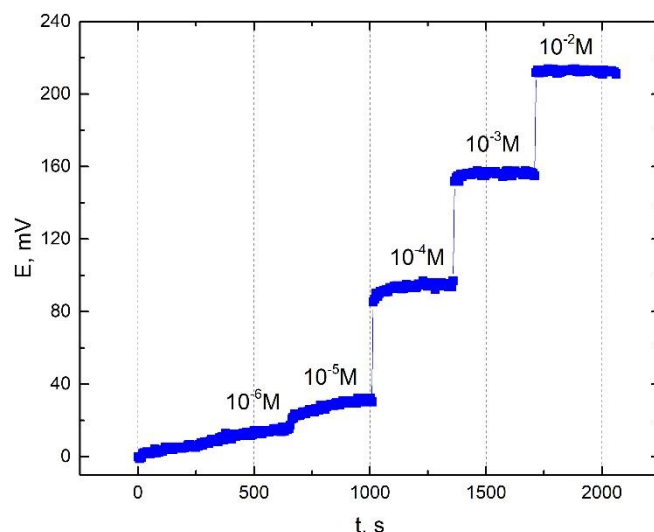


Figure 4. Typical response time curve for sensor *L10* in Cs^+ solutions.

4. Conclusions

Novel ligands based on functionalized pillar[5]arenes were synthesized and structurally characterized. The performance of the new ligands as receptors in potentiometric sensors with plasticized polymeric membranes was explored in details for the first time. The sensitivity was assessed in aqueous solutions of alkali, alkali earth, transition metals and lanthanides. The influence of membrane components (solvent plasticizer and cation exchanger) was established. The ligands *P3* and *P4* on average gave the highest sensitivity to alkali metals and ammonium. In case of alkali earth metals, the best response was obtained from *P1*-based sensors. The same holds for transition metals, however, in this

case the difference between *P1*- and *P4*-based sensors was not that pronounced. Selectivity studies indicated that the developed ligands show no sharp selectivity towards particular ions but provide a broad cross-sensitivity in certain groups of metals depending on the pillar[5]arene structure, and can be employed in potentiometric multisensor arrays as they show cross-sensitivity patterns different from those described in the literature for other types of sensors.

Supplementary Materials: The following supporting information can be downloaded at: <https://www.mdpi.com/article/10.3390/chemosensors10100420/s1>, Figure S1. FT-IR spectrum of P2; Figure S2. FT-IR spectrum of P4; Figure S3. FT-IR spectrum of P5; Figure S4. ¹H-NMR spectrum of P2; Figure S5. ¹³C-NMR spectrum of P2; Figure S6. ¹H-NMR spectrum of P4; Figure S7. ¹³C-NMR spectrum of P4; Figure S8. ¹H-NMR spectrum of P5; Figure S9. ¹³C-NMR spectrum of P5; Figure S10. 3D PCA score plot; Figure S11. pH-sensitivity of the pillar[5]arene based potentiometric sensors. Table S1. Average sensitivities of the sensors calculated for all studied ions.

Author Contributions: Conceptualization, D.K. and A.N.K.; methodology, D.K. and A.N.K.; software, D.K. and E.Y.; validation, D.K. and A.N.K.; formal analysis, M.D., E.Y. and D.K.; investigation, M.D., E.Y. and A.N.K.; resources, D.K. and A.N.K.; writing—original draft preparation, M.D., E.Y., A.N.K. and D.K.; writing—review and editing, D.K. and A.N.K.; visualization, M.D., E.Y. and D.K.; supervision, D.K.; project administration, D.K. All authors have read and agreed to the published version of the manuscript.

Funding: This research received no external funding.

Institutional Review Board Statement: Not applicable.

Informed Consent Statement: Not applicable.

Data Availability Statement: Data are contained within the article and supplementary material.

Conflicts of Interest: The authors declare no conflict of interest.

References

1. Ogoshi, T.; Kanai, S.; Fujinami, S.; Yamagishi, T.A.; Nakamoto, Y. Para-bridged symmetrical pillar[5]arenes: Their Lewis acid catalyzed synthesis and host-guest property. *J. Am. Chem. Soc.* **2008**, *130*, 5022–5023. [[CrossRef](#)]
2. Ogoshi, T.; Yamagishi, T.A.; Nakamoto, Y. Pillar-shaped macrocyclic hosts pillar[n]arenes: New key players for supramolecular chemistry. *Chem. Rev.* **2016**, *116*, 7937–8002. [[CrossRef](#)] [[PubMed](#)]
3. Cragg, P.J.; Sharma, K. Pillar[5]arenes: Fascinating cyclophanes with a bright future. *Chem. Soc. Rev.* **2012**, *41*, 597–607. [[CrossRef](#)]
4. Xue, M.; Yang, Y.; Chi, X.; Zhang, Z.; Huang, F. Pillararenes, a new class of macrocycles for supramolecular chemistry. *Acc. Chem. Res.* **2012**, *45*, 1294–1308. [[CrossRef](#)]
5. Holler, M.; Allenbach, N.; Sonet, J.; Nierengarten, J.F. The high yielding synthesis of pillar[5]arenes under Friedel-Crafts conditions explained by dynamic covalent bond formation. *Chem. Commun.* **2012**, *48*, 2576–2578. [[CrossRef](#)] [[PubMed](#)]
6. Li, H.; Quan, K.; Yang, X.; Li, Z.; Zhao, L.; Qiu, H. Recent developments for the investigation of chiral properties and applications of pillar[5]arenes in analytical chemistry. *TrAC-Trends Anal. Chem.* **2020**, *131*, 116026. [[CrossRef](#)]
7. Liu, X.; Jia, K.; Wang, Y.; Shao, W.; Yao, C.; Peng, L.; Zhang, D.; Hu, X.Y.; Wang, L. Dual-responsive bola-type supra-amphiphile constructed from water-soluble pillar[5]arene and naphthalimide-containing amphiphile for intracellular drug delivery. *ACS Appl. Mater. Interfaces* **2017**, *9*, 4843–4850. [[CrossRef](#)] [[PubMed](#)]
8. Sun, G.; He, Z.; Hao, M.; Zuo, M.; Xu, Z.; Hu, X.Y.; Zhu, J.J.; Wang, L. Dual acid-responsive bola-type supramolecular vesicles for efficient intracellular anticancer drug delivery. *J. Mater. Chem. B* **2019**, *7*, 3944–3949. [[CrossRef](#)]
9. Wang, Y.; Du, J.; Wang, Y.; Jin, Q.; Ji, J. Pillar[5]arene based supramolecular prodrug micelles with pH induced aggregate behavior for intracellular drug delivery. *Chem. Commun.* **2015**, *51*, 2999–3002. [[CrossRef](#)]
10. Yang, K.; Pei, Y.; Wen, J.; Pei, Z. Recent advances in pillar[n]arenes: Synthesis and applications based on host-guest interactions. *Chem. Commun.* **2016**, *52*, 9316–9326. [[CrossRef](#)] [[PubMed](#)]
11. Cragg, P.J. Pillar[n]arenes at the chemistry-biology interface. *Isr. J. Chem.* **2018**, *58*, 1158–1172. [[CrossRef](#)]
12. Dube, L.E.; Patel, B.A.; Fagan-murphy, A.; Kothur, R.R.; Cragg, P.J. Detection of clinically important cations by a pillar[5]arene-modified electrochemical sensor. *Chem. Sens.* **2013**, *3*, 1–6.
13. Zhang, Y.M.; He, J.X.; Zhu, W.; Li, Y.F.; Fang, H.; Yao, H.; Wei, T.B.; Lin, Q. Novel pillar[5]arene-based supramolecular organic framework gel for ultrasensitive response Fe³⁺ and F[−] in water. *Mater. Sci. Eng. C* **2019**, *100*, 62–69. [[CrossRef](#)] [[PubMed](#)]
14. Fang, Y.; Yuan, X.; Wu, L.; Peng, Z.; Feng, W.; Liu, N.; Xu, D.; Li, S.; Sengupta, A.; Mohapatra, P.K.; et al. Ditopic CMPO-pillar[5]arenes as unique receptors for efficient separation of americium(iii) and europium(iii). *Chem. Commun.* **2015**, *51*, 4263–4266. [[CrossRef](#)]

15. Yang, Q.Y.; Zhang, Y.M.; Ma, X.Q.; Dong, H.Q.; Zhang, Y.F.; Guan, W.L.; Yao, H.; Wei, T.B.; Lin, Q. A pillar[5]arene-based fluorescent sensor for sensitive detection of L-Met through a dual-site collaborative mechanism. *Spectrochim. Acta A Mol. Biomol. Spectrosc.* **2020**, *240*, 118569. [[CrossRef](#)] [[PubMed](#)]
16. Chen, Y.Y.; Gong, G.F.; Zhang, Y.M.; Fan, Y.Q.; Guan, X.W.; Zhou, Q.; Yang, H.L.; Yao, H.; Wei, T.B.; Lin, Q. A novel pillar[5]arene-based chemosensor for dual-channel detecting L-Arg by multiple supramolecular interactions. *Dye. Pigment.* **2019**, *171*, 107706. [[CrossRef](#)]
17. Wu, L.; Fang, Y.; Jia, Y.; Yang, Y.; Liao, J.; Liu, N.; Yang, X.; Feng, W.; Ming, J.; Yuan, L. Pillar[5]arene-based diglycolamides for highly efficient separation of americium(III) and europium(III). *Dalt. Trans.* **2014**, *43*, 3835–3838. [[CrossRef](#)] [[PubMed](#)]
18. Li, C.; Wu, L.; Chen, L.; Yuan, X.; Cai, Y.; Feng, W.; Liu, N.; Ren, Y.; Sengupta, A.; Murali, M.S.; et al. Highly efficient extraction of actinides with pillar[5]arene-derived diglycolamides in ionic liquids via a unique mechanism involving competitive host-guest interactions. *Dalt. Trans.* **2016**, *45*, 19299–19310. [[CrossRef](#)]
19. Yuan, X.; Cai, Y.; Chen, L.; Lu, S.; Xiao, X.; Yuan, L.; Feng, W. Phosphine oxides functionalized pillar[5]arenes for uranyl extraction: Solvent effect and thermodynamics. *Sep. Purif. Technol.* **2020**, *230*, 11584. [[CrossRef](#)]
20. Yakimova, L.S.; Shurpik, D.N.; Makhmutova, A.R.; Stoikov, I.I. Pillar[5]arenes bearing amide and carboxylic groups as synthetic receptors for alkali metal ions. *Macroheterocycles* **2017**, *10*, 226–232. [[CrossRef](#)]
21. Lin, Q.; Zheng, F.; Liu, L.; Mao, P.P.; Zhang, Y.M.; Yao, H.; Wei, T.B. Efficient sensing of fluoride ions in water using a novel water soluble self-assembled supramolecular sensor based on pillar[5]arene. *RSC Adv.* **2016**, *6*, 111928–111933. [[CrossRef](#)]
22. Wei, T.B.; Cheng, X.B.; Li, H.; Zheng, F.; Lin, Q.; Yao, H.; Zhang, Y.M. A Novel functionalized pillar[5]arene: Synthesis, assembly and application in sequential fluorescent sensing for Fe³⁺ and F[−] in aqueous media. *RSC Adv.* **2016**, *6*, 20987–20993. [[CrossRef](#)]
23. Ma, X.Q.; Wang, Y.; Wei, T.B.; Qi, L.H.; Jiang, X.M.; Ding, J.D.; Zhu, W.B.; Yao, H.; Zhang, Y.M.; Lin, Q. A novel AIE chemosensor based on quinoline functionalized Pillar[5]arene for highly selective and sensitive sequential detection of toxic Hg²⁺ and CN[−]. *Dye. Pigment.* **2019**, *164*, 279–286. [[CrossRef](#)]
24. Shamagsumova, R.V.; Shurpik, D.N.; Padnya, P.L.; Stoikov, I.I.; Evtugyn, G.A. Acetylcholinesterase biosensor for inhibitor measurements based on glassy carbon electrode modified with carbon black and pillar[5]arene. *Talanta* **2015**, *144*, 559–568. [[CrossRef](#)]
25. Smolko, V.A.; Shurpik, D.N.; Shamagsumova, R.V.; Porfireva, A.V.; Evtugyn, V.G.; Yakimova, L.S.; Stoikov, I.I.; Evtugyn, G.A. Electrochemical behavior of pillar[5]arene on glassy carbon electrode and its interaction with Cu²⁺ and Ag⁺ ions. *Electrochim. Acta* **2014**, *147*, 726–734. [[CrossRef](#)]
26. Sun, J.; Guo, F.; Shi, Q.; Wu, H.; Sun, Y.; Chen, M.; Diao, G. Electrochemical detection of paraquat based on silver nanoparticles/water-soluble pillar[5]arene functionalized graphene oxide modified glassy carbon electrode. *J. Electroanal. Chem.* **2019**, *847*, 113221. [[CrossRef](#)]
27. Stoikova, E.E.; Sorvin, M.I.; Shurpik, D.N.; Budnikov, H.C.; Stoikov, I.I.; Evtugyn, G.A. Solid-contact potentiometric sensor based on polyaniline and unsubstituted pillar[5]arene. *Electroanalysis* **2015**, *27*, 440–449. [[CrossRef](#)]
28. Kothur, R.R.; Hall, J.; Patel, B.A.; Leong, C.L.; Boutelle, M.G.; Cragg, P.J. A low pH sensor from an esterified pillar[5]arene. *Chem. Commun.* **2014**, *50*, 852–854. [[CrossRef](#)]
29. Acikbas, Y.; Aksoy, M.; Aksoy, M.; Karaagac, D.; Bastug, E.; Kursunlu, A.N.; Erdogan, M.; Capan, R.; Ozmen, M.; Ersoz, M. Recent progress in pillar[n]arene-based thin films on chemical sensor applications. *J. Incl. Phenom. Macrocycl. Chem.* **2021**, *100*, 39–54. [[CrossRef](#)]
30. Zinin, A.I.; Stepanova, E.V.; Jost, U.; Kondakov, N.N.; Shpirt, A.M.; Chizhov, A.O.; Torgov, V.I.; Kononov, L.O. An efficient multigram-scale synthesis of 4-(ω-chloroalkoxy)phenols. *Russ. Chem. Bull.* **2017**, *66*, 304–312. [[CrossRef](#)]
31. Kursunlu, A.N.; Acikbas, Y.; Ozmen, M.; Erdogan, M.; Capan, R. Fabrication of LB thin film of pillar[5]arene-2-amino-3-hydroxypyridine for the sensing of vapors. *Mater. Lett.* **2020**, *267*, 127538. [[CrossRef](#)]
32. Bastug, E.; Kursunlu, A.N.; Guler, E. A fluorescent clever macrocycle: Deca-bodipy bearing a pillar [5]arene and its selective binding of asparagine in half-aqueous medium. *J. Lumin.* **2020**, *225*, 117343. [[CrossRef](#)]
33. Bro, R.; Smilde, A.K. Principal component analysis. *Anal. Methods* **2014**, *6*, 2812–2831. [[CrossRef](#)]
34. Kursunlu, A.; Baslak, C. A Bodipy-bearing pillar[5]arene for mimicking photosynthesis: Multi-fluorophoric light harvesting system. *Tetrahed. Lett.* **2018**, *59*, 1958–1962. [[CrossRef](#)]
35. Kursunlu, A.; Acikbas, Y.; Ozmen, M.; Erdogan, M.; Capan, R. Haloalkanes and aromatic hydrocarbons sensing using Langmuir-Blodgett thin film of pillar[5]arene-biphenylcarboxylic acid. *Colloids Surf. A Physicochem. Eng. Asp.* **2019**, *565*, 108–117. [[CrossRef](#)]
36. Ciosek, P.; Wróblewski, W. Sensor arrays for liquid sensing—Electronic tongue systems. *Analyst* **2007**, *132*, 963–978. [[CrossRef](#)]
37. Bratov, A.; Abramova, N.; Ipatov, A. Recent trends in potentiometric sensor arrays—A review. *Anal. Chim. Acta* **2010**, *678*, 149–159. [[CrossRef](#)]
38. Mimendia, A.; Gutiérrez, J.M.; Leija, L.; Hernández, P.R.; Favari, L.; Muñoz, R.; del Valle, M. A review of the use of the potentiometric electronic tongue in the monitoring of environmental systems. *Environ. Model. Software* **2010**, *25*, 1023–1030. [[CrossRef](#)]
39. Geană, E.I.; Ciucure, C.T.; Apetrei, C. Electrochemical sensors coupled with multivariate statistical analysis as screening tools for wine authentication issues: A review. *Chemosensors* **2020**, *8*, 59. [[CrossRef](#)]

40. Parshina, A.; Kolganova, T.; Safronova, E.; Osipov, A.; Lapshina, E.; Yelnikova, A.; Bobreshova, O.; Yaroslavtsev, A. Perfluorosulfonic acid membranes thermally treated and modified by dopants with proton-acceptor properties for asparaginate and potassium ions determination in pharmaceuticals. *Membranes* **2019**, *9*, 142. [[CrossRef](#)]
41. Khaydukova, M.; Militsyn, D.; Karnaukh, M.; Grüner, B.; Selucký, P.; Babain, V.; Wilden, A.; Kirsanov, D.; Legin, A. Modified diamide and phosphine oxide extracting compounds as membrane components for cross-sensitive chemical sensors. *Chemosensors* **2019**, *7*, 41. [[CrossRef](#)]
42. Yaroshenko, I.; Kirsanov, D.; Kartsova, L.; Sidorova, A.; Borisova, I.; Legin, A. Determination of urine ionic composition with potentiometric multisensor system. *Talanta* **2015**, *131*, 556–561. [[CrossRef](#)] [[PubMed](#)]